Electronic Structure of Face- and Edge-Shared Bioctahedral Systems: A Comparison of $M_2Cl_9^{3-}$ and $M_2Cl_{10}^{4-}$, M = Cr, Mo, W

John E. McGrady, Robert Stranger,* and Timothy Lovell

Department of Chemistry, The Faculties, The Australian National University, Canberra, ACT 0200, Australia

Received May 9, 1997

Potential energy curves for the broken-symmetry states of the edge-shared bimetallic systems, $M_2Cl_{10}^{4-}$ (M = Cr, Mo, W), are analyzed using approximate density functional theory. The potential energy curves are made up of distinct sections, depending on which subsets of metal-based electrons are localized or delocalized. Starting from the fully delocalized limit, the metal-based electrons localize in the order δ before π before σ as the metal−metal separation is progressively increased. As a result there are four distinct regions of the potential energy curve, corresponding to (a) $\sigma + \pi + \delta$ delocalized; (b) $\sigma + \pi$ delocalized, δ localized; (c) σ delocalized, $\pi + \delta$ localized; and (d) $\sigma + \pi + \delta$ localized. Localization of the δ subset of electrons is particularly facile, because interactions with the bridging ligands destabilize the δ orbital relative to δ^*. As a result, at metal−metal separations greater than approximately 2.30 Å, delocalization of the δ electrons would result in formation of a M−M antibond rather than a bond. For $Cr_2Cl_{10}^{4-}$, the fully localized region of the curve lies much lower than the others, but for the molybdenum and tungsten congeners, all four regions lie within 1.0 eV of each other, giving rise to complex and relatively flat potential energy curves. The decahalides of the chromium triad therefore exhibit the well-established trend toward greater delocalization in complexes of the heavier transition metals. This trend is, however, found to be far less prominent than in the face-shared analogues, $M_2Cl_9^{3-}$, and the difference between the two structural types is traced to the inability of the edge-shared bridge to support the short metal−metal separations necessary for complete electron delocalization.

Introduction

In recent years the chemistry of systems containing two or more transition metal centers has expanded rapidly.[1] Small clusters of metal atoms have obvious applications in the study of metal surfaces,[2] electronic devices,[3] and catalysts,[4] as well as the relatively new discipline of bioinorganic chemistry.[5] For example, the oxygen-transport proteins hemerythrin[6] and hemocyanin[7] feature diiron and dicopper sites, respectively, while manganese catalase contains two manganese ions.[8] More complex polymetallic active sites are also known, notably the manganese cluster in the oxygen-evolving complex (OEC) of photosystem II[9] and the sulfide-bridged iron clusters which play a central role in a variety of electron transport processes.[10] The precise role played by the polymetallic active site in these systems remains to be determined, but it seems clear that the presence of more than one metal center, coupled in a specific manner, may provide an electronic environment uniquely suited to catalyzing a specific reaction.

The appreciation of the general importance of bimetallic sites, along with the synthesis of a vast array of model complexes, has been accompanied by advances in the understanding of their electronic structure, particularly with reference to the nature of the metal−metal interactions.[1] In this respect, it is important to distinguish two distinct categories of complexes, those with an unsupported metal−metal bond, and those in which the metal centers are spanned by one or more bridging groups. While an unsupported dimer necessarily relies on the direct overlap of metal-based orbitals for its stability, bridged systems may be stabilized solely by covalent interactions between metal and bridging atoms and, hence, do not necessarily require the presence of a strong metal−metal bond. As a result, the presence of bridging ligands introduces great flexibility, and the metal−metal bonding within a series of bridged dimers may vary enormously depending on the nature of the metal and ligands.

Systems based on two octahedrally coordinated metal centers are particularly common, and they include examples where one, two (edge-shared), or three (face-shared) ligands are found in bridging positions. Within the series of face-shared nonachlorides,[11] metal−metal interactions span a continuum from strong triple bonding (exemplified by $W_2Cl_9^{3-}$) to nonbonding ($Cr_2Cl_9^{3-}$). Metal−metal separations reflect this spectrum,

(1) Cotton, F. A.; Walton, R. A. *Multiple Bonds Between Metal Atoms*; Oxford University Press: Oxford, U.K., 1993 and references therein.
(2) Neurock, M.; van Santen, R. A.; Biemolt, W.; Jansen, A. P. J. *J. Am. Chem. Soc*. **1994**, *116*, 6860.
(3) McGhee, E. M.; Godfrey, M. R.; Hoffman, B. M.; Ibers, J. A. *Inorg. Chem*. **1991**, *30*, 803.
(4) (a) Koga, N.; Morokuma, K. *Chem. Rev*. **1991**, *91*, 823. (b) Neyman, K. M.; Nasluzov, V. A.; Hahn, J.; Landis, C. R.; Rösch, N. *Organometallics* **1997**, *16*, 995.
(5) Holm, R. H.; Kennepohl, P.; Solomon, E. I. *Chem. Rev.* **1996**, *96*, 2239 and references therein.
(6) Holmes, M. A.; LeTrong, I.; Turley, S.; Sieker, L. C.; Stenkamp, R. E. *J. Mol. Biol.* **1991**, *218*, 583.
(7) Magnus, K.; Ton-That, H. *J. Inorg. Biochem.* **1992**, *47*, 20.
(8) Gamelin, D. R.; Kirk, M. L.; Stemmler, T. L.; Pal, S.; Armstrong, W. H.; Penner-Hahn, J. E.; Solomon, E. I. *J. Am. Chem. Soc*. **1994**, *116*, 2392.
(9) Brudvig, G. W.; Thorp, H. H.; Crabtree, R. H. *Acc. Chem. Res*. **1991**, *24*, 311.
(10) Sykes, A. G. *Met. Ions Biol. Syst*. **1991**, *27*, 291.
(11) Cotton, F. A.; Ucko, D. A. *Inorg. Chim. Acta* **1972**, *6*, 161.

S0020-1669(97)00553-3 CCC: $15.00
Published on Web 07/10/1998

varying from approximately 2.40 Å for the tungsten system[12] to in excess of 3.1 Å for the dichromium analogue.[13] The general class of edge-shared complexes show a similar diversity of structure and bonding,[14] but unfortunately the subgroup of homoleptic decahalides, $M_2X_{10}^{z-}$, is far less diverse than its nonahalide counterpart. Neutral[15] and anionic[16] systems with a variety of d electron counts are known, but where structural data are available, metal−metal separations are without exception long, the shortest being the 3.63 Å Os−Os separation observed in $Os_2Cl_{10}^{2-}$.[16a] However, the structurally characterized systems represent only a small subgroup of known complexes, and there remains a real possibility that adjustment of oxidation state may induce significant metal−metal bonding in the decahalides. In this respect it is interesting to note that stepwise reduction of $Os_2Br_{10}^{z-}$ results in the loss of bromide and the formation of $Os_2Br_9^{(z-1)-}$,[17] which features a direct Os−Os bond. It may be that reduction-induced changes in the metal−metal bonding in the decabromide complex facilitate the expulsion of the halide and adoption of the face-shared architecture. Similar redox-linked structural changes may be a feature of the reactivity of the enzymatic active sites mentioned above, which often involve the binding, chemical modification, and expulsion of small molecules at the active sites.

We have recently discussed in detail the potential energy curves of face-shared bioctahedral systems[18−20] using approximate density functional theory. The initial focus was placed on complexes with the d^3d^3 electronic configuration, followed more recently by an analysis of other configurations,[21] where the degeneracy (or near-degeneracy) of the metal-based orbitals complicates the potential energy curves considerably. It is the purpose of this paper to provide a similar analysis of the related edge-shared bioctahedra. We again focus on model systems with the simple d^3d^3 configuration, exemplified by the decachlorides of the chromium triad, $M_2Cl_{10}^{4-}$ (M = Cr, Mo, W). Unfortunately none of these complexes are known, although the isoelectronic $Tc_2Cl_{10}^{2-}$ complex has recently been reported.[16f] Nevertheless, the simplicity of the analysis, along with the resultant comparison with the corresponding series of nonachlorides, which holds a central position in the chemistry of the face-shared systems, justifies the choice of model systems.

In order to discuss periodic trends in metal−metal interactions, it is clearly necessary to be able to accurately describe weak antiferromagnetic coupling at the same level of theory as the opposite extreme of strong metal−metal bonding. As in previous work, we therefore make extensive use of the broken-symmetry methodology developed by Noodleman and coworkers,[22] which provides a means of treating weakly interacting electrons in a physically realistic manner. The method relies on removing all symmetry elements connecting the two metal ions (symmetry breaking), thereby allowing (but not forcing) electrons of opposite spins to localize on opposite centers. The spin singlet ground state then arises through weak antiferromagnetic coupling rather than strong bonding. The broken-symmetry methodology has been used to calculate ground-state electronic structures and magnetic properties of a variety of bimetallic systems[23] and, more recently, to optimize structural parameters.[18−21,23l,24] If, in contrast, the two sides of the molecule are constrained to be symmetry-equivalent, the metal-based electrons are forced to delocalize over both sides of the molecule, a situation which is clearly realistic only in the presence of a relatively strong metal−metal bond. This can lead to underestimation of metal−metal separations by as much as 1.0 Å in weakly coupled systems such as $Cr_2Cl_9^{3-}$.[18] It is important to emphasize that the two extremes described above (localized electrons, antiferromagnetic coupling; delocalized electrons, strong metal−metal bonding) represent two limits of a continuum of intermediate bonding situations, all of which are encompassed by the broken-symmetry methodology.

Computational Details

All approximate density functional[25] calculations reported in this work were performed using the Amsterdam Density Functional (ADF) program, version 2.0.1.[26] A double-ζ Slater type orbital basis set extended with a single d-polarization function was used to describe chlorine, while all metals were modeled with triple-ζ basis sets. Electrons in orbitals up to and including 2p {Cl}, 3p {Cr}, 4p {Mo}, and 5p {W} were considered to be part of the core and treated in accordance with the frozen-core approximation. All broken-symmetry calculations were performed in C_{3v} (face-shared) or C_{2v} (edge-shared) symmetry, and an asymmetry in the initial spin density was introduced using the "modifystartpotential" key. The corresponding full-symmetry calculations were performed in D_{3h} and D_{2h} symmetry, respectively.

(12) (a) Dunbar, K. R.; Pence, L. E. *Acta Crystallogr.* **1991**, *C47*, 23. (b) Watson, W. H., Jr.; Waser, J. *Acta Crystallogr.* **1958**, *11*, 689. (c) Stranger, R.; Grey, I. E.; Madsen, I. C.; Smith, P. W. *J. Solid State Chem.* **1987**, *69*, 162.

(13) (a) Saillant, R.; Wentworth, R. A. D. *Inorg. Chem.* **1968**, *7*, 1606. (b) Wessel, G. J.; Ijdo, D. J. W. *Acta Crystallogr.* **1957**, *10*, 466. (c) Grey, I. E.; Smith, P. W. *Aust. J. Chem.* **1971**, *24*, 73.

(14) Cotton, F. A. *Polyhedron* **1987**, *6*, 667.

(15) (a) Zalkin, A.; Sands, D. E. *Acta Crystallogr.* **1958**, *11*, 615. (b) Sands, D. E.; Zalkin, A. *Acta Crystallogr.* **1959**, *12*, 723. (c) Cotton, F. A.; Rice, C. E. *Acta Crystallogr.* **1978**, *B34*, 2833. (d) Mucker, K.; Smith, G. S.; Johnson, Q. *Acta Crystallogr.* **1968**, *B24*, 874.

(16) (a) Eicher, J.; Klingelhöfer, P.; Müller, U.; Dehnicke, K. *Z. Anorg. Allg. Chem.* **1984**, *514*, 79. (b) Kistenmacher, T. J.; Stucky, G. P. *Inorg. Chem.* **1971**, *10*, 122. (c) Eicher, J.; Müller, U.; Dehnicke, K. *Z. Anorg. Allg. Chem.* **1985**, *521*, 37. (d) Hey, E.; Weller, F.; Dehnicke, K. *Z. Anorg. Allg. Chem.* **1984**, *508*, 86. (e) Schmidt, I.; Patt-Siebel, U.; Müller, U.; Dehnicke, K. *Z. Anorg. Allg. Chem.* **1988**, *556*, 57. (f) Wendt, A.; Preetz, W. *Z. Anorg. Allg. Chem.* **1994**, *620*, 655. (g) Calderazzo, F.; Pallavicini, P.; Pampaloni, G.; Zanazzi, P. F. *J. Chem. Soc., Dalton Trans.* **1990**, 2743. (h) Krebs, B.; Henckel, G.; Dartmann, M.; Preetz, W.; Bruns, M. *Z. Naturforsch.* **1984**, *39b*, 843. (i) Bruns, M.; Preetz, W. *Z. Anorg. Allg. Chem.* **1986**, *537*, 88. (j) Cotton, F. A.; Duraj, S. A.; Hinckley, C. C.; Matusz, M.; Roth, W. J. *Inorg. Chem.* **1984**, *23*, 3080. (k) Hollmann, P.; Preetz, W. *Z. Naturforsch.* **1992**, *47b*, 1115. (l) Hollmann, P.; Preetz, W. *Z. Anorg. Allg. Chem.* **1991**, *601*, 47.

(17) Heath, G. A.; Humphrey, D. G. *Chem. Commun.* **1990**, 672.

(18) Lovell, T.; McGrady, J. E.; Stranger, R.; Macgregor, S. A. *Inorg. Chem.* **1996**, *35*, 3079.

(19) McGrady, J. E.; Stranger, R.; Lovell, T. *J. Phys. Chem. A* **1997**, *101*, 6265.

(20) McGrady, J. E.; Stranger, R.; Lovell, T. *Inorg. Chem.* **1997**, *36*, 3242.

(21) Stranger, R.; McGrady, J. E.; Lovell, T. Submitted to *Inorg. Chem.*

(22) (a) Noodleman, L.; Norman, J. G. *J. Chem. Phys.* **1979**, *70*, 4903. (b) Noodleman, L. *J. Chem. Phys.* **1981**, *74*, 5737.

(23) (a) Medley, G. A.; Stranger, R. *Inorg. Chem.* **1994**, *33*, 3976. (b) Brown, C. A.; Remar, G. J.; Musselman, R. L.; Solomon, E. I. *Inorg. Chem.* **1995**, *34*, 688. (c) Mouesca, J.-M.; Chen, J. L.; Noodleman, L.; Bashford, D.; Case, D. A. *J. Am. Chem. Soc.* **1994**, *116*, 11898. (d) Noodleman, L.; Case, D. A. *Adv. Inorg. Chem.* **1992**, *38*, 423. (e) Jacobsen, H.; Kraatz, H. B.; Ziegler, T.; Boorman, P. M. *J. Am. Chem. Soc.* **1992**, *114*, 7851. (f) Ross, P. K.; Solomon, E. I. *J. Am. Chem. Soc.* **1991**, *113*, 3246. (g) Bencini, A. Gatteschi, D. *J. Am. Chem. Soc.* **1986**, *108*, 5763. (h) Noodleman, L.; Baerends, E. J. *J. Am. Chem. Soc.* **1984**, *106*, 2316. (i) Aizman, A.; Case, D. A. *J. Am. Chem. Soc.* **1982**, *104*, 3269. (j) Andzelm, J.; Wimmer, E. *J. Chem. Phys.* **1992**, *96*, 1280. (k) Zhao, X. G.; Richardson, W. H.; Chen, J.-L.; Noodleman, L.; Tsai, H.-L.; Hendrickson, D. N. *Inorg. Chem.* **1997**, *36*, 1198. (l) McGrady, J. E.; Stranger, R. *J. Am. Chem. Soc.* **1997**, *119*, 8512.

(24) (a) Edgecombe, K. E.; Becke, A. D. *Chem. Phys. Lett.* **1995**, *244*, 427. (b) Delley, B.; Freeman, A. J.; Ellis, D. E. *Phys. Rev. Lett.* **1985**, *54*, 661. (c) Baykara, N. A.; McMaster, B. N.; Salahub, D. R. *Mol. Phys.* **1984**, *52*, 891. (d) Dunlap, B. I. *Phys. Rev. A* **1983**, *27*, 2217. (e) Ziegler, T.; Tschinke, V.; Becke, A. *Polyhedron* **1987**, *6*, 685.

(25) Ziegler, T. *Chem. Rev.* **1991**, *91*, 651.

(26) (a) Baerends, E. J.; Ellis, D. E.; Ros, P. *Chem. Phys.* **1973**, *2*, 42. (b) Baerends, E. J.; Ros, P. *Int. J. Quantum Chem.* **1978**, *S12*, 169. (c) te Velde, G.; Baerends E. J. *J. Comput. Phys.* **1992**, *99*, 84.

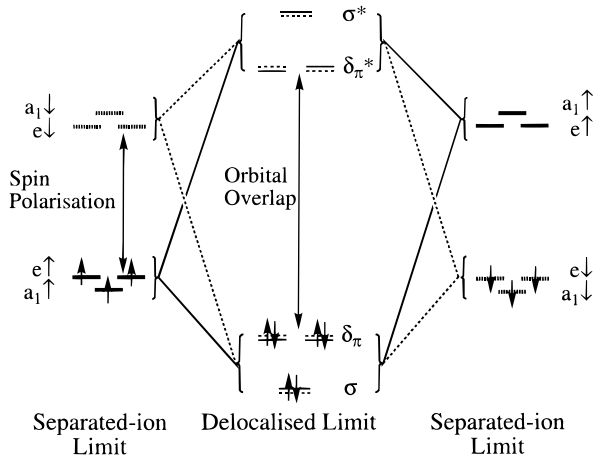

Figure 1. Representation of the broken-symmetry state of $M_2Cl_9^{3-}$: both delocalized and separated-ion limits are shown. Orbitals are labeled according to the representations of the C_{3v} point group.

No attempt was made to use approximate spin-projection techniques to obtain the energy of the true ground state as we have illustrated in a previous publication that, where such projection is valid, it makes negligible difference to the shape of the potential energy curve.[19] The LDA approximation, including the local exchange-correlation potential of Vosko, Wilk, and Nusair,[27] was employed throughout. Neither gradient nor quasi-relativistic corrections were considered as they have been shown to result in generally poorer agreement with the crystallographically determined structures than the LDA in isolation. The individual points on the potential energy curves were calculated by freezing the metal−metal separation, r_{M-M}, and optimizing all other independent structural parameters using the gradient algorithm of Versluis and Ziegler.[28]

Results

Face-Shared Systems, $M_2Cl_9^{3-}$. We and other authors have described the electronic structures of bimetallic systems linked by a triple halide bridge in detail elsewhere,[18−21,29] and so only the features of the bonding most relevant to the comparison with their edge-shared analogues will be discussed here. Each metal center has local trigonal symmetry, and consequently the t_{2g}-based orbitals are split into subsets of a_1 and e symmetry, which respectively have σ and δ_π symmetry with respect to the metal−metal axis. For an isolated single ion with a d^3 configuration, each of these orbitals is singly occupied, with the electron spins parallel, giving a spin-quartet state. As a result the majority-spin metal-based orbitals lie significantly lower than their minority-spin, vacant counterparts (see Figure 1, separated-ion limit).

The process of metal−metal bond formation may be regarded as a progressive delocalization of the metal-based orbitals over both centers. In the limit of weak metal−metal interactions, each electron remains essentially localized on one side or another, and the spin singlet ground state arises through antiparallel (antiferromagnetic) coupling of the spins on opposite centers. In this case, the metal−metal coupling is best regarded as a small perturbation on the energy level scheme of two isolated single ions. As the orbitals become progressively more delocalized, two major changes occur. First, the spin density at each center is lowered, thereby reducing the spin polarization splitting; second, the orbitals gain significant bonding or antibonding character. In the limit of full delocalization, the single-ion orbitals of a_1 symmetry give rise to σ bonding and antibonding orbitals (a_1' and a_2'', respectively, in D_{3h} symmetry) while the single-ion e orbitals give rise to δ_π bonding and antibonding orbitals (e′ and e″ symmetry, respectively). The splittings within the energy level scheme in Figure 1 therefore arise from very different sources, depending on the extent of delocalization: at the separated-ion (weakly coupled) limit, spin polarization is responsible for the separation between the occupied and vacant orbitals, whereas at the delocalized limit, orbital overlap causes a splitting between bonding and antibonding pairs.

Without making any assumptions regarding the localization of the orbitals, or their bonding or antibonding character, the broken-symmetry state can always be defined, using labels from the C_{3v} point group, by the configuration $(a_1\uparrow)^1(a_1\downarrow)^1(e\uparrow)^2(e\downarrow)^2$-$(e\uparrow)^0(e\downarrow)^0(a_1\uparrow)^0(a_1\downarrow)^0$. As noted above, in the weakly coupled limit the separation between occupied and vacant orbitals arises through spin polarization, whereas in the strongly coupled limit, the separation arises through orbital overlap. In principle, there are four distinct ways in which the broken-symmetry state defined above may be attained, depending on which subsets of electrons are involved in weak magnetic coupling (localized) or strong metal−metal bonding (delocalized): (a) all electrons delocalized; (b) σ delocalized, δ_π localized; (c) σ localized, δ_π delocalized; and (d) all localized. The simplest way to determine which description is appropriate at any point on the curve is to consider the associated states, $S = 0$, 1, 2, and 3. For these states the orbitals are labeled according to the full D_{3h} molecular symmetry because in each case the electrons are found to be fully delocalized, even in the absence of symmetry elements connecting the two metal centers.

If, in the broken-symmetry state, all metal-based electrons are localized and therefore weakly antiferromagnetically coupled, then the associated state where all metal-based electrons are decoupled, $S = 3$, defined as $(a_1'\uparrow)^1(a_1'\downarrow)^0(e'\uparrow)^2(e'\downarrow)^0(e''\uparrow)^2(e''\downarrow)^0$-$(a_2''\uparrow)^1(a_2''\downarrow)^0$, will lie close in energy. Likewise, if the σ orbitals are delocalized in the broken-symmetry state, but their δ_π counterparts remain weakly coupled, then the $S = 2$ state, $(a_1'\uparrow)^1(a_1'\downarrow)^1(e'\uparrow)^2(e'\downarrow)^0(e''\uparrow)^2(e''\downarrow)^0(a_2''\uparrow)^0(a_2''\downarrow)^0$, where only the δ_π electrons are uncoupled, will lie closest in energy. Similar logic suggests that if only the σ electrons are weakly coupled, the $S = 1$ state, $(a_1'\uparrow)^1(a_1'\downarrow)^0(e'\uparrow)^2(e'\downarrow)^2(e''\uparrow)^0(e''\downarrow)^0(a_2''\uparrow)^1(a_2''\downarrow)^0$, corresponding to the uncoupling of the σ electrons in isolation, will lie close to the broken-symmetry state. Finally, if all metal-based orbitals are delocalized, then the broken-symmetry state is identical to the singlet ground state obtained from a calculation performed in full D_{3h} symmetry. This state, denoted $S = 0$, is defined by the configuration $(a_1'\uparrow)^1(a_1'\downarrow)^1(e'\uparrow)^2(e'\downarrow)^2(e''\uparrow)^0(e''\downarrow)^0$-$(a_2''\uparrow)^0(a_2''\downarrow)^0$. It is important to emphasize the distinction between this $S = 0$ state, where full electron delocalization is forced on the electrons, and the broken-symmetry state, which also has a net spin of 0, but where no prior assumption regarding the localization/delocalization of the electrons is made. Throughout the following discussion, the reader should bear in mind that the ground state is always the antiferromagnetic broken-symmetry state, and the energies of the associated spin states are emphasized only because they provide a convenient means of breaking down the potential energy curves into distinct segments.

Curves for the broken-symmetry and associated states ($S = 0$, 1, 2, and 3) are shown in Figure 2 for $M_2Cl_9^{3-}$, M = Cr, Mo, W. In all cases, the broken-symmetry ground state (bold) passes smoothly from the minima in the $S = 0$ state to $S = 2$ and then $S = 3$ as the metal−metal separation increases ($S = 0$ is not shown for $Cr_2Cl_9^{3-}$, as its minimum lies over 3 eV

(27) Vosko, S. H.; Wilk, L.; Nusair, M. *Can. J. Phys.* **1980**, *58*, 1200.
(28) Versluis, L.; Ziegler, T. *J. Chem. Phys.* **1988**, *88*, 322.
(29) Summerville, R. H.; Hoffmann, R. *J. Am. Chem. Soc.* **1979**, *101*, 3821.

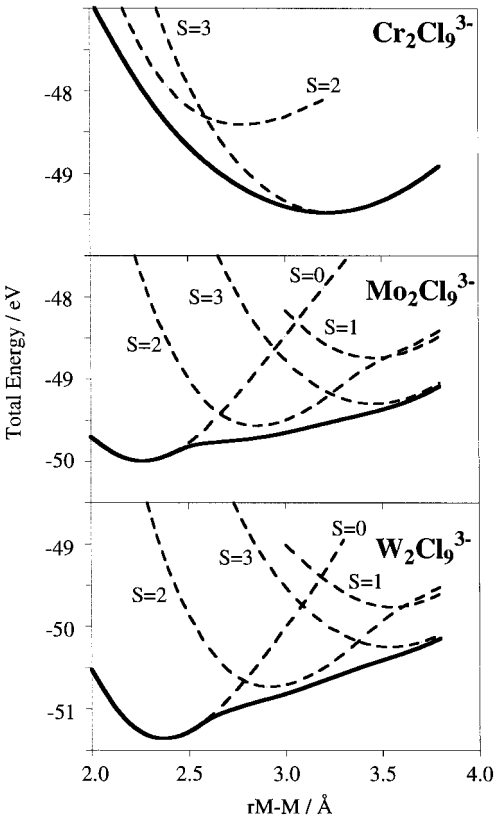

Figure 2. Potential energy curves for the broken-symmetry and $S = 0$, 1, 2, and 3 associated states of $M_2X_9^{3-}$ (M = Cr, Mo, W).

higher than that for the broken-symmetry state). In contrast, the $S = 1$ state lies well above the broken-symmetry curve at all metal−metal separations. These observations indicate that as the metal−metal separation increases, the broken-symmetry state passes through three distinct regions corresponding to the situations a, b, and d described above. The situation described by c, where the σ electrons are localized but their δ_π counterparts are delocalized, is never a valid description of the broken-symmetry state, because the associated $S = 1$ state lies too high in energy at all points on the curve. This simply confirms the intuitive expectation that the σ electrons always delocalize before their δ_π counterparts. We also note that only over the range of metal−metal separations where the potential energy curves for the associated states converge or lie parallel and close to the broken-symmetry curve will the calculated energies for the associated states correspond closely to the true spin multiplet energies. Finally, because the broken-symmetry state closely follows the minima in the $S = 0$, 2, and 3 associated states, the global minimum in the broken-symmetry curve for any particular complex is simply determined by which of the three associated states lies lowest in energy. Thus where $S = 0$ lies lowest ($W_2Cl_9^{3-}$ and $Mo_2Cl_9^{3-}$), the ground-state metal−metal separation is short and all electrons are delocalized, whereas for $Cr_2Cl_9^{3-}$, $S = 3$ lies lowest, all metal-based electrons are localized, and the Cr−Cr separation is large.

Edge-Shared Systems, $Mo_2Cl_{10}^{4-}$. In the edge-shared systems, the local symmetry at each metal center is C_{2v} and so the degeneracy of the t_{2g} manifold is entirely lifted, giving orbitals of a_1, b_2, and a_2 symmetry (Figure 3, separated-ion limit). Coupling between the two ions results in a broken-symmetry state defined by $(a_1\uparrow)^1(a_1\downarrow)^1(b_2\uparrow)^1(b_2\downarrow)^1(a_2\uparrow)^1(a_2\downarrow)^1(a_2\uparrow)^0(a_2\downarrow)^0(b_2\uparrow)^0(b_2\downarrow)^0(a_1\uparrow)^0(a_1\downarrow)^0$, where the labels of the C_{2v} point group indicate that once again no prior assumption has been made regarding the localization/delocalization of the electrons. At the fully

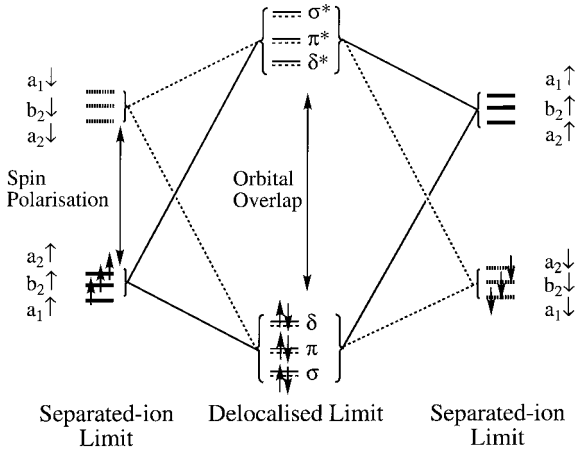

Figure 3. Representation of the broken-symmetry state of $Mo_2Cl_{10}^{4-}$: orbitals are labeled according to the representations of the C_{2v} point group.

delocalized limit, the single-ion a_1, b_2, and a_2 orbitals combine to give metal−metal bonding/antibonding combinations of σ, π, and δ symmetry, respectively.[30] The completely localized and delocalized extremes bear many qualitative similarities to those in the face-shared analogues, but at intermediate separations, the presence of symmetry-distinct σ, π, and δ orbitals leads to a more complex potential curve. There are now six intermediate bonding situations between the fully localized and delocalized limits (compared to two in the face-shared systems), depending on the order in which the different subsets of electrons localize. Including the two limiting cases, there are therefore eight possible descriptions of the broken-symmetry state, and to determine which description is the most appropriate at any point, we must consider the associated states, summarized in Table 1. Again, full D_{2h} symmetry is used to describe these states since, analogous to the associated states in $M_2Cl_9^{3-}$, they are found to be fully delocalized.

The broken-symmetry potential energy curve for $Mo_2Cl_{10}^{4-}$ is shown in Figure 4, along with the eight associated states $S = 0$, $S = 1^{a-c}$, $S = 2^{a-c}$, and $S = 3$. The broken-symmetry curve follows smoothly from $S = 0$ (rMo−Mo < 2.2 Å) via $S = 1^a$ (rMo−Mo < 3.0 Å), $S = 2^a$ (rMo−Mo < 3.4 Å), to $S = 3$ (rMo−Mo > 3.4 Å). The remaining four states, $S = 1^{b,c}$ and $S = 2^{b,c}$, lie considerably higher in energy than the broken-symmetry state at all points. Thus the broken-symmetry potential energy curve can be subdivided into four distinct regions: (a) where rMo−Mo < 2.2 Å, all metal-based electrons are delocalized; (b) where 2.2 < rMo−Mo < 3.0 Å, $\sigma + \pi$ are delocalized and δ is localized; (c) where 3.0 < rMo−Mo < 3.4 Å, σ is delocalized and $\pi + \delta$ are localized; (d) where rMo−Mo > 3.4 Å, all metal-based electrons are localized. Once again, we note that only where the curves for the associated states converge or lie parallel and close to the broken-symmetry curve will the calculated energies for the associated states correspond closely to the true spin multiplet energies. The high energies of the $S = 1^{b,c}$ and $S = 2^{b,c}$ states confirm that the electrons localize in the order δ before π before σ, as might have been anticipated on the basis of simple orbital overlap arguments. In the case of $Mo_2Cl_{10}^{4-}$, the $S = 3$ state lies lowest, and hence the global minimum in the broken-symmetry state is found at large rMo−Mo (4.1 Å), where all metal-based electrons are completely localized. The ground state is therefore distinctly different from that of the isovalent face-shared species, $Mo_2Cl_9^{3-}$,

(30) Shaik, S.; Hoffmann, R.; Fisel, C. R.; Summerville, R. H. *J. Am. Chem. Soc.* **1980**, *102*, 4555.

Table 1. Associated States for Various Regions of the Broken-Symmetry Potential Energy Curves for M_2X_9 and M_2X_{10} Complexes with the d^3d^3 Configuration

broken-symmetry region		
delocalized	localized	associated state
		M_2X_9
$\sigma + \delta_\pi$	none	$S = 0$ $(a_1'^{\uparrow})^1(a_1'^{\downarrow})^1(e'^{\uparrow})^2(e'^{\downarrow})^2(e''^{\uparrow})^0(e''^{\downarrow})^0(a_2''^{\uparrow})^0(a_2''^{\downarrow})^0$
δ_π	σ	$S = 1$ $(a_1'^{\uparrow})^1(a_1'^{\downarrow})^0(e'^{\uparrow})^2(e'^{\downarrow})^2(e''^{\uparrow})^0(e''^{\downarrow})^0(a_2''^{\uparrow})^1(a_2''^{\downarrow})^0$
σ	δ_π	$S = 2$ $(a_1'^{\uparrow})^1(a_1'^{\downarrow})^1(e'^{\uparrow})^2(e'^{\downarrow})^0(e''^{\uparrow})^2(e''^{\downarrow})^0(a_2''^{\uparrow})^0(a_2''^{\downarrow})^0$
none	$\sigma + \delta_\pi$	$S = 3$ $(a_1'^{\uparrow})^1(a_1'^{\downarrow})^0(e'^{\uparrow})^2(e'^{\downarrow})^0(e''^{\uparrow})^2(e''^{\downarrow})^0(a_2''^{\uparrow})^1(a_2''^{\downarrow})^0$
		M_2X_{10}
$\sigma + \pi + \delta$	none	$S = 0$ $(a_g{\uparrow})^1(a_g{\downarrow})^1(b_{2u}{\uparrow})^1(b_{2u}{\downarrow})^1(b_{1g}{\uparrow})^1(b_{1g}{\downarrow})^1(a_u{\uparrow})^0(a_u{\downarrow})^0(b_{3g}{\uparrow})^0(b_{3g}{\downarrow})^0(b_{1u}{\uparrow})^0(b_{1u}{\downarrow})^0$
$\sigma + \pi$	δ	$S = 1^a$ $(a_g{\uparrow})^1(a_g{\downarrow})^1(b_{2u}{\uparrow})^1(b_{2u}{\downarrow})^1(b_{1g}{\uparrow})^1(b_{1g}{\downarrow})^0(a_u{\uparrow})^1(a_u{\downarrow})^0(b_{3g}{\uparrow})^0(b_{3g}{\downarrow})^0(b_{1u}{\uparrow})^0(b_{1u}{\downarrow})^0$
$\sigma + \delta$	π	$S = 1^b$ $(a_g{\uparrow})^1(a_g{\downarrow})^1(b_{2u}{\uparrow})^1(b_{2u}{\downarrow})^0(b_{1g}{\uparrow})^1(b_{1g}{\downarrow})^1(a_u{\uparrow})^0(a_u{\downarrow})^0(b_{3g}{\uparrow})^1(b_{3g}{\downarrow})^0(b_{1u}{\uparrow})^0(b_{1u}{\downarrow})^0$
$\pi + \delta$	σ	$S = 1^c$ $(a_g{\uparrow})^1(a_g{\downarrow})^0(b_{2u}{\uparrow})^1(b_{2u}{\downarrow})^1(b_{1g}{\uparrow})^1(b_{1g}{\downarrow})^1(a_u{\uparrow})^0(a_u{\downarrow})^0(b_{3g}{\uparrow})^0(b_{3g}{\downarrow})^0(b_{1u}{\uparrow})^1(b_{1u}{\downarrow})^0$
σ	$\pi + \delta$	$S = 2^a$ $(a_g{\uparrow})^1(a_g{\downarrow})^1(b_{2u}{\uparrow})^1(b_{2u}{\downarrow})^0(b_{1g}{\uparrow})^1(b_{1g}{\downarrow})^0(a_u{\uparrow})^1(a_u{\downarrow})^0(b_{3g}{\uparrow})^1(b_{3g}{\downarrow})^0(b_{1u}{\uparrow})^0(b_{1u}{\downarrow})^0$
π	$\sigma + \delta$	$S = 2^b$ $(a_g{\uparrow})^1(a_g{\downarrow})^0(b_{2u}{\uparrow})^1(b_{2u}{\downarrow})^1(b_{1g}{\uparrow})^1(b_{1g}{\downarrow})^0(a_u{\uparrow})^1(a_u{\downarrow})^0(b_{3g}{\uparrow})^0(b_{3g}{\downarrow})^0(b_{1u}{\uparrow})^1(b_{1u}{\downarrow})^0$
δ	$\sigma + \pi$	$S = 2^c$ $(a_g{\uparrow})^1(a_g{\downarrow})^0(b_{2u}{\uparrow})^1(b_{2u}{\downarrow})^0(b_{1g}{\uparrow})^1(b_{1g}{\downarrow})^1(a_u{\uparrow})^0(a_u{\downarrow})^0(b_{3g}{\uparrow})^1(b_{3g}{\downarrow})^0(b_{1u}{\uparrow})^1(b_{1u}{\downarrow})^0$
none	$\sigma + \pi + \delta$	$S = 3$ $(a_g{\uparrow})^1(a_g{\downarrow})^0(b_{2u}{\uparrow})^1(b_{2u}{\downarrow})^0(b_{1g}{\uparrow})^1(b_{1g}{\downarrow})^0(a_u{\uparrow})^1(a_u{\downarrow})^0(b_{3g}{\uparrow})^1(b_{3g}{\downarrow})^0(b_{1u}{\uparrow})^1(b_{1u}{\downarrow})^0$

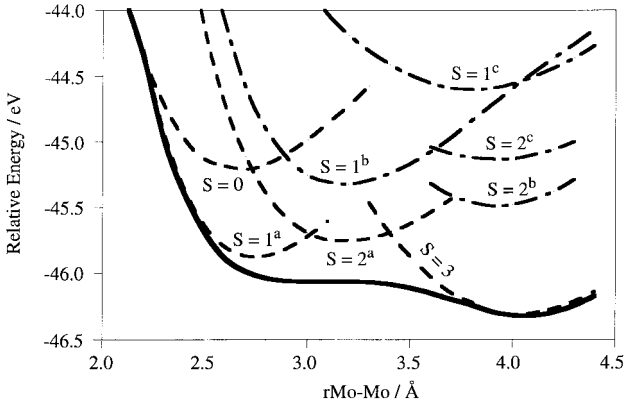

Figure 4. Potential energy curves for the broken-symmetry and $S = 0$, 1^{a-c}, 2^{a-c}, and 3 associated states of $Mo_2Cl_{10}^{4-}$.

in which all metal-based electrons are delocalized, and the Mo−Mo separation is short.

A particularly significant feature of Figure 4 is the relative positions of the minima in the $S = 0$ and $S = 1^a$ curves. For the $S = 0$, 2, and 3 states in the $Mo_2Cl_9^{3-}$ system (Figure 2), there is a steady increase in the metal−metal separation as the electrons are successively decoupled, but for $Mo_2Cl_{10}^{4-}$ the minimum in the $S = 1^a$ curve (where the δ electrons are decoupled) lies almost directly below that in $S = 0$. In terms of the broken-symmetry ground state, this implies that the [$\sigma + \pi$ delocalized, δ localized] region is more stable than its fully delocalized counterpart down to very short metal−metal separations (2.2 Å), and only below this point do the δ electrons delocalize. This situation contrasts markedly with the δ_π electrons of $Mo_2Cl_9^{3-}$ which delocalize at metal−metal separations of approximately 2.6 Å. The reluctance of the δ electrons to delocalize can be linked to the well-established inversion of the δ and δ^* orbitals.[30] In the limit of full delocalization (D_{2h} symmetry), there is an occupied orbital localized on the bridging $\{Cl_2\}$ array of correct symmetry to overlap with the δ orbital, but not one to match its antibonding δ^* counterpart. As a result, interactions with the bridge destabilize δ relative to δ^*, and only where *r*Mo−Mo < 2.2 Å do through-space interactions dominate, and the normal δ below δ^* ordering returns. This means that, at separations greater than 2.2 Å, delocalization of the δ electrons would lead to the formation of a Mo−Mo antibond and is therefore unfavorable. The net result of the inversion of δ and δ^* is therefore to make the δ electrons very difficult to delocalize and force the [$\sigma + \pi$ delocalized, δ localized] bonding situation to persist over an unusually wide range of metal−metal separations.

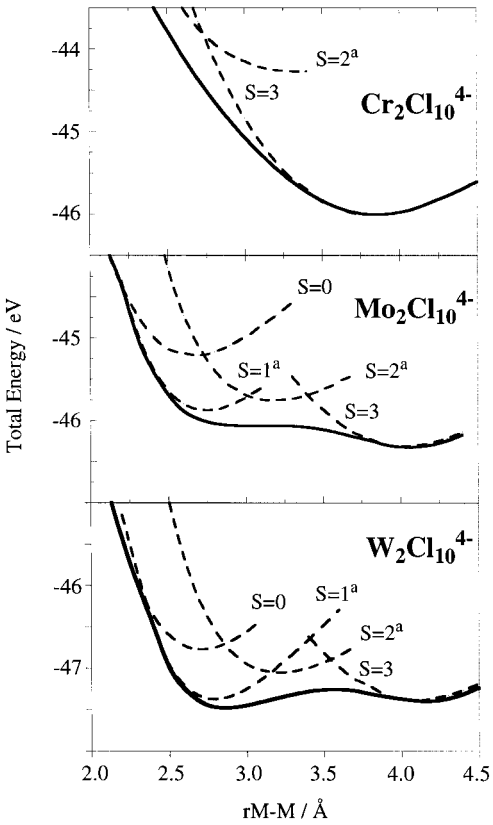

Figure 5. Potential energy curves for the broken-symmetry and $S = 0$, 1^a, 2^a, and 3 associated states of $M_2X_{10}^{4-}$ (M = Cr, Mo, W).

Potential energy curves for the broken-symmetry states of $Cr_2Cl_{10}^{4-}$, $Mo_2Cl_{10}^{4-}$, and $W_2Cl_{10}^{4-}$ are shown in Figure 5, along with the associated states $S = 0$, 1^a, 2^a, and 3. The remaining associated states, $S = 1^{b,c}$ and $2^{b,c}$, lie well above the broken-symmetry curve in all cases and are omitted for clarity. The $Cr_2Cl_{10}^{4-}$ complex is the simplest of the three to describe, because the $S = 3$ state lies almost 2 eV lower than any of the others. The position of the global minimum in the broken-symmetry state is therefore clear: all metal-based electrons are completely localized and the Cr−Cr separation is long. The potential energy curves for systems containing second- and third-row transition metals are rather more complex, because all four associated states lie within 1.0 eV of the global minimum. For $Mo_2Cl_{10}^{4-}$, the most stable of the four is $S = 3$, giving rise to the localized ground state noted above, but both the $S = 1^a$ and $S = 2^a$ states lie less than 0.5 eV higher. As a

result, a distinct plateau emerges over the range 2.8 Å < *r*Mo−Mo < 3.4 Å, where the $S = 1^a$ and $S = 2^a$ states lie closest to the curve, this plateau lying only 0.25 eV above the fully localized ground state. The delocalization of the σ and π electrons is therefore associated with only a small loss in energy. Similar features emerged in the potential energy curve for $Mo_2Cl_9^{3-}$, the geometry of which is notably dependent on the size of the countercation. It is therefore likely that if the $Mo_2Cl_{10}^{4-}$ anion could be synthesized, its structure would also be highly sensitive to the surrounding crystal environment and could potentially display Mo−Mo separations ranging between 2.8 Å and 4.1 Å.

In $W_2Cl_{10}^{4-}$, the $S = 0$, 1^a, and 2^a states are all further stabilized relative to $S = 3$, and as a result the $S = 1^a$ and $S = 3$ states are almost equienergetic, and the potential energy curve exhibits two distinct minima separated by 1.6 Å. The minimum at *r*W−W = 4.20 Å corresponds to full localization of all electrons, while at *r*W−W = 2.6 Å the σ and π electrons are delocalized, giving rise to an effective W−W double bond. The presence of two distinct minima raises the interesting possibility that bond-length isomerism may be possible in the $W_2Cl_{10}^{4-}$ anion, but as the barrier between the two minima is rather small (0.2 eV), it is more likely that the anion would simply exhibit strong cation dependence.

Within the series of edge-shared complexes, we once again note the well-established periodic trend toward greater delocalization in the complexes of the second and third transition series elements. It is, however, clear from a comparison of Figures 2 and 5 that the delocalization of the metal-based electrons is less favored in the edge-shared systems. Thus, while the chromium systems are completely localized regardless of the bridging architecture, the transition from face- to edge-sharing causes a dramatic change in metal−metal bonding in the molybdenum and tungsten complexes. Whereas both $Mo_2Cl_9^{3-}$ and $W_2Cl_9^{3-}$ have delocalized ground states, with $S = 0$ clearly lower than $S = 3$, the ordering of the two associated states is reversed for $Mo_2Cl_{10}^{4-}$ and $W_2Cl_{10}^{4-}$. A quantitative estimate of the position of the localization/delocalization equilibrium may therefore be obtained simply from the relative energies of the $S = 0$ and $S = 3$ states, which represent the delocalized and localized limits, respectively. In a recent publication[20] we used this concept to gain insight into the underlying electronic reasons for the observed periodic trends. In the following section, we extend the analysis to the edge-shared species and compare and contrast the two structural types.

Analysis of the Localization/Delocalization Equilibria in $M_2Cl_9^{3-}$ and $M_2Cl_{10}^{4-}$. We noted above that the tendency of the electrons to delocalize is determined simply by the relative energies of the $S = 0$ and $S = 3$ states. Thus if the $S = 3$ state lies lower than $S = 0$, then the electrons will localize in the ground state, whereas the reverse ordering indicates that delocalization will be favored. In order to gain independent estimates of the energies of the $S = 0$ and $S = 3$ states, a common reference point is required (Figure 6). For the face-shared systems, a convenient reference state may be defined by the configuration $(a_1'\uparrow)^{0.5}(a_1'\downarrow)^{0.5}(e'\uparrow)^1(e'\downarrow)^1(e''\uparrow)^1(e''\downarrow)^1(a_2''\uparrow)^{0.5}$-$(a_2''\downarrow)^{0.5}$, which differs from $S = 0$ only in that it has no net bond, and from $S = 3$ only in that it has no spin polarization. The $(a_g\uparrow)^{0.5}(a_g\downarrow)^{0.5}(b_{2u}\uparrow)^{0.5}(b_{2u}\downarrow)^{0.5}(b_{1g}\uparrow)^{0.5}(b_{1g}\downarrow)^{0.5}(a_u\uparrow)^{0.5}(a_u\downarrow)^{0.5}$-$(b_{3g}\uparrow)^{0.5}(b_{3g}\downarrow)^{0.5}(b_{1u}\uparrow)^{0.5}(b_{1u}\downarrow)^{0.5}$ configuration provides a parallel reference point for the edge-shared systems. The separation of the reference and $S = 3$ states (ΔE_{spe}) measures the sum of the spin polarization energies associated with the two isolated d^3 single ions, whereas the separation of reference and $S = 0$ states

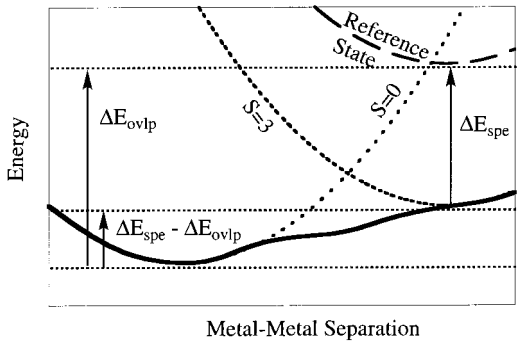

Figure 6. Schematic representation of the potential energy curves for the $S = 0$, $S = 3$, and reference states.

Table 2. Overlap and Spin Polarization Energies (eV) for MCl_6^{3-}, $M_2Cl_9^{3-}$, and $M_2Cl_{10}^{4-}$ Complexes[a]

complex	ΔE_{ovlp}	ΔE_{spe}	$\Delta E_{spe} - \Delta E_{ovlp}$	complex	single-ion SPE
$[Cr_2Cl_9]^{3-}$	+1.02	+3.55	+2.53	$[CrCl_6]^{3-}$	+1.86
$[Mo_2Cl_9]^{3-}$	+2.88	+2.19	−0.69	$[MoCl_6]^{3-}$	+1.14
$[W_2Cl_9]^{3-}$	+3.10	+2.00	−1.10	$[WCl_6]^{3-}$	+1.03
$[Cr_2Cl_{10}]^{4-}$	−0.04	+3.62	+3.66		
$[Mo_2Cl_{10}]^{4-}$	+1.15	+2.25	+1.10		
$[W_2Cl_{10}]^{4-}$	+1.48	+2.04	+0.62		

[a] See text for definition of terms.

(ΔE_{ovlp}) measures the energy associated with formation of a triple bond. The difference between the two terms, $\Delta E_{spe} - \Delta E_{ovlp}$, is simply the separation of the $S = 0$ and $S = 3$ states. Within the series of face-shared systems, analysis on this basis indicates that changes in both overlap (ΔE_{ovlp}) and spin polarization energy (ΔE_{spe}) contributed approximately equally to the overall trend toward greater delocalization of electrons in the complexes of the heavier metals.[20]

The two terms defined in Figure 6, ΔE_{spe} and ΔE_{ovlp}, and their difference, $\Delta E_{spe} - \Delta E_{ovlp}$, are summarized in Table 2 for the edge-shared and face-shared complexes of the chromium triad. Single-ion spin polarization energies for the monomeric hexachlorides are also shown for comparison. The most striking feature of Table 2 is the insensitivity of the ΔE_{spe} term to the bridging architecture. In both face- and edge-shared systems, ΔE_{spe} is approximately equal to twice the relevant single-ion spin polarization energy, indicating that, at the localized limit, the ions are effectively independent of each other. Therefore, on going from the face-shared to edge-shared systems, changes in $\Delta E_{spe} - \Delta E_{ovlp}$ are caused almost entirely by changes in the ΔE_{ovlp} term, i.e., by changes in the stability of the $S = 0$ state, not $S = 3$.

The reasons for this difference become clear if we consider the steric requirements of the face- and edge-shared structures in the absence of metal−metal bonding. Potential energy curves for dirhodium complexes, $Rh_2Cl_9^{3-}$ and $Rh_2Cl_{10}^{4-}$, where the d^6 configuration of the Rh^{3+} ion precludes any metal−metal bonding, are compared in Figure 7. The minimum in the face-shared system occurs approximately 0.55 Å before that in the edge-shared system, an observation which is simply related to the geometric requirements of the bridges. Assuming a representative Rh−Cl_{br} bond length of 2.44 Å, the metal−metal separation in a perfect face-shared bioctahedron, where all the bond angles are 90°, is 2.82 Å, while that in the analogous edge-shared system is 3.45 Å. The optimized Rh−Rh separations are somewhat longer, at 3.22 and 3.77 Å, due to the repulsion between the tripositive cations, but the difference between the

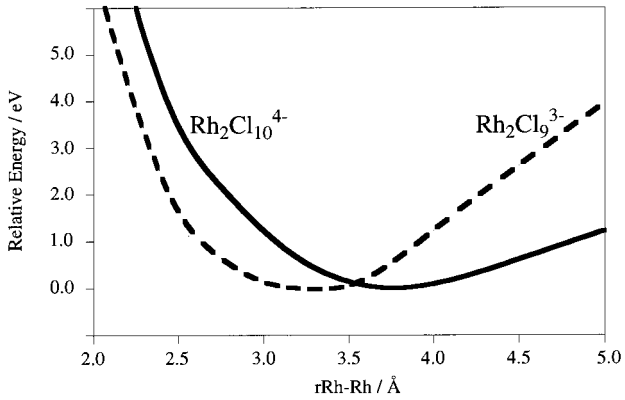

Figure 7. Comparison of the potential energy curves for $Rh_2Cl_9^{3-}$ and $Rh_2Cl_{10}^{4-}$. The minimum in each curve is taken as the zero of energy in each case.

two (0.55 Å) compares favorably with the idealized separation of 0.63 Å.

The potential energy curves shown in Figures 2 and 5 may be regarded as arising from a superposition of the effects of metal−metal bonding on an underlying potential energy curve determined by the steric requirements of the bridge. Considering first the $S = 3$ state, we note that the principal stabilizing influence is the single-ion spin polarization energy, which is essentially independent of the metal−metal separation. The positions of the minima in the $S = 3$ curves are therefore determined primarily by the steric requirements of the bridge, and the 0.5 Å difference between edge- and face-shared systems persists. In contrast, the energy of the $S = 0$ state is strongly dependent on the metal−metal separation, with optimal overlap of metal-based orbitals occurring at relatively short metal−metal separations. In this region, the potential energy for $Rh_2Cl_{10}^{4-}$ is rising rapidly as a consequence of the steric requirements of the bridge, but that for $Rh_2Cl_9^{3-}$ remains relatively close to the minimum. Therefore, while both face- and edge-shared architectures are sufficiently flexible to allow the metal-based electrons to localize completely, only the face-shared motif can support the short metal−metal separations necessary to promote complete electron delocalization.

Summary

In this paper we have analyzed potential energy curves for the broken-symmetry states of $M_2Cl_{10}^{4-}$ (M = Cr, Mo, and W) and compared the results with the corresponding data for the face-shared systems, $M_2Cl_9^{3-}$. In the face-shared systems, metal-based electrons of σ symmetry delocalize before their δ_π counterparts, whereas in the edge-shared systems, the order of delocalization is σ before π before δ. These trends are fully in accord with the expectations based on the overlap of the metal-based orbitals. The δ electrons of the edge-shared complexes are found to resist delocalization even at very short metal−metal separations, due to interactions with the bridging ligand orbitals which destabilize δ relative to δ^*. As a result, at metal−metal separations greater than approximately 2.20 Å, delocalization would result in the formation of a metal−metal antibond rather than a bond. Both face- and edge-shared systems display the well-established periodic trend toward greater delocalization in complexes of the heavier transition metals, but the tendency to delocalize is much reduced in the edge-shared systems. The difference between the two structural types is traced to the inability of the edge-shared bridge to allow the close approach of metal ions required to stabilize the fully delocalized states.

Acknowledgment. We express our gratitude to the Australian Research Council (ARC) for financial support and the EPSRC (U.K.) for a scholarship to T.L.

IC970553J